Phase space analysis of networks based on biologically realistic parameters

Nicole Voges *, Laurent Perrinet

Institut de Neurosciences Cognitives de la Méditerranée, UMR6193 CNRS – Aix-Marseille Université, Marseille, France

ARTICLE INFO

ABSTRACT

We study cortical network dynamics for a spatially embedded network model. It represents, in terms of spatial scale, a large piece of cortex allowing for long-range connections, resulting in a rather sparse connectivity. The spatial embedding also permits us to include distance-dependent conduction delays. We use two different types of conductance-based I&F neurons as excitatory and inhibitory units, as well as specific connection probabilities. In order to remain computationally tractable, we reduce neuron density, modelling part of the missing internal input via external poissonian spike trains. Compared to previous studies, we observe significant changes in the dynamical phase space: Altered activity patterns require another regularity measures than the coefficient of variation. Hence, we compare three different regularity measure on the basis of artificial inter-spike-interval distributions. We identify two types of mixed states, where different phases coexist in certain regions of the phase space. More notably, our boundary between high and low activity states depends predominantly on the relation between excitatory and inhibitory synaptic strength instead of the input rate.

© 2009 Elsevier Ltd. All rights reserved.

1. Introduction

Studying cortical network dynamics on the basis of artificial neural networks requires an appropriate simplification of the system. The latter should be adapted to cortical reality but remain tractable for simulations. There is a plethora of detailed information about how to model a cortical network, in addition to a set of appropriate analysis tools. For example, Brunel (2000) examined the phase space of sparsely connected neuronal networks with current-based synapses, Kumar et al. (2008a) advanced to conductance-based synapses, and Roxin et al. (2005) focussed on synaptic delays. The benefits of such studies are, for example, the detection of stable ground states, showing which dynamical states occur under what conditions, and they are most advantageous in identifying the most sensitive parameters. We present an elaborate analysis of the dynamical states of a 2D spatially embedded cortical network. Compared to previous studies on the dynamics of randomly connected cortical networks (Brunel, 2000; Kumar et al., 2008a; Roxin et al., 2005) we focus on a biologically realistic spatial embedding. It is the aim of this paper to provide first insights into the behavior of such a network.

Despite the fact that cortical connectivity is distance-dependent (Binzegger et al., 2007; Voges, 2007), we still consider random networks, but with three important modifications.

First, we assume a much sparser connectivity than most models (see Kumar et al., 2008b; Mehring et al., 2003). These studies are focused on a local scale of about 1 mm side length, where around 10% of all possible connections are realized. In reality, however, approximately half of the synapses of most pyramidal neurons are established to cells that are located at a distance more than 0.5 mm away (Binzegger et al., 2007; Buzas et al., 2006). We enlarged the spatial scale, so that each neuron is connected to a much smaller fraction of all other neurons within the network. Assuming a spatial scale of 5 mm side length results in a connectivity of about 1% instead of 10. The spatial base enables us to consider distance-dependent conduction delays. The disadvantage of such a setting is a strongly reduced and therefore unrealistic neuron density which must be compensated for by external input assumptions.

Second, we consider specific connection probabilities for the synapses established between excitatory (exc.) and inhibitory (inh.) neurons. In purely randomly wired networks (Brunel, 2000; Kumar et al., 2008a) the numeric relation between the number of exc.–exc. (ee), exc.–inh. (ei), inh.–exc. (ie) and inh.–inh. (ii) synapses is merely defined by the corresponding frequencies of exc. and inh. neurons. We base our network model on the realistic connection probabilities provided by Binzegger et al. (2004), which describes layers 2/3 in cat primary visual cortex.

Third, with respect to cortical physiology (Muller, 2003; Nowak et al., 2003), we consider two different types of conductance-based integrate-and-fire (I&F) neurons, namely fast spiking inh. and regular spiking exc. neurons. Since most of the quantities characterizing the phase space are directly related to the dynamical properties of a neuron, e.g. the mean firing rate, we calculate them separately for the two populations. We examine if the two populations exhibit

* Corresponding author.
E-mail address: Nicole.Voges@incm.cnrs-mrs.fr (N. Voges).

Table 1
List of parameters that define exc. and inh. neurons. Identical for both populations are the resting membrane potential V_{rest}, the reset potential V_{reset}, and the spiking threshold V_{θ}. Differing parameters are the synaptic time constants $\tau^{e,i}$, the reversal potentials $V_{rev}^{e,i}$, the membrane capacitances $C_m^{e,i}$, and the membrane conductances at rest $G_{rest}^{e,i}$. The latter two reflect the passive electrical properties of the membrane at rest leading to the membrane time constants $\tau_{rest}^{e,i} = C_m^{e,i}/G_{rest}^{e,i}$, i.e., fast spiking inh. and regular spiking exc. neurons.

Type	V_{rest}, V_{reset} (mV)	V_{θ} (mV)	τ (ms)	V_{rev} (mV)	C_m (pF)	G_{rest} (nS)	τ_{rest} (ms)
Exc.	−70	−55	1.5	0	289.5	29	10
Inh.	−70	−55	10	−80	141	21.2	6.7

significantly different activities which would prevent averaging over exc. and inh. neurons.

Following Brunel (2000) and Kumar et al. (2008a), we systematically vary the excitation–inhibition ratio together with the external input rate every neuron receives. The question is whether the resulting phase space differs from previously published ones: what are the changes in terms of possible activity patterns? Do new critical parameters emerge due to the new assumptions? In particular, we investigate the effect of our modifications on the transitions between different activity states.

Characterizing the resulting network activities, we realized that the typical measure to describe regularity in neuronal spiking, the coefficient of variation, *CV*, is not appropriate for much of our simulated data. To handle the occurrence of multimodal inter-spike-interval distributions and very low firing rates we evaluate two additional quantities, the so-called 'local *CV*', and a measure that is based on the Kullback–Leibler information, CV_{KL} (Kostal and Lansky, 2006; Koyama and Shinomoto, 2007). In order to justify and validate the use of CV_{KL}, we compare the results of these three regularity measures for several artificial distributions. We also estimate the number of samples needed to correctly describe the irregularity of a poissonian spike train. The necessity of this analysis is based on the limited simulation time which, in a sense, corresponds to limited trial times in biological experiments.

In the next section, we introduce and explain the network and the simulations that are based on it. Then, we define the measures we use to characterize the dynamical states in network activity. Finally, we elaborate and discuss the simulation results: the advantage of using CV_{KL}, the changes in network activity compared to previous studies, and, in particular, the relation between specific, cortically inspired parameters and the real cortical network.

2. Methods

We consider $N = 49,163$ I&F neurons (Gerstner and Kistler, 2002; Tuckwell, 1988) that are quasi-randomly distributed in a 2D quadratic domain with periodic boundary conditions.[1] Following Binzegger et al. (2004) we assume 22% inh. cell types (104^2 neurons arranged on jittered lattice positions), and 78% exc. pyramidal cells (($104^2/0.22$) ∗ 0.78 neurons with uniformly distributed spatial positions). The global connectivity of this model is $c = \bar{k}/N \approx 0.0153$, with an average number $\bar{k} \simeq 752$ in- and out-going synapses per neuron. Instead of assuming merely random connections (60.84% ee, 17.16% ei and ie, and 4.84% ii synapses), our networks comprise 71.1% ee, 9.96% ei, 16.14% ie and 2.8% ii synapses. Compared to Kumar et al. (2008a) and Mehring et al. (2003) the spatial region covered here represents a larger piece of cortex than the usually assumed 1×1 mm^2: at the expense of an unrealistically small neuron density, we model a cortical sheet of 5×5 mm^2.

Differing from Brunel (2000) we use conductance-based I&F neurons similar to those in Kumar et al. (2008a,b), but with two different types of neurons: regular spiking exc. cells and fast spiking inh. cells, similar to Brunel and Wang (2003), Muller (2003), and Nowak et al. (2003). The two neuron populations and their synaptic time constants are defined by the parameters listed in

---

[1] Using this number and type of neuron, we can easily compare our results with (Kumar et al., 2008a).

Table 1. The strength of a synapse is given by its peak amplitude J^e, J^i of the conductance transient. All internal synapses have a distance-dependent conduction delay calculated for an average conduction velocity of 1.5 m/s for neurons closer than 0.15 mm and 3 m/s for larger distances (representing myelinated axons). In addition, we assume a general synaptic conduction delay, randomly and uniformly chosen from [1.2,1.5] ms.

Each exc. neuron receives external poissonian input at a rate v_{ext} while inh. neurons receive rates reduced by a factor $f_i = 0.66$, such that $v_i = v_{ext} \cdot f_i$. The exc. synaptic weights are drawn from a Gaussian distribution ($\sigma = 10\%$ of μ) to produce EPSPs of on average 0.11 mV peak amplitude in exc. and 0.28 mV peak amplitude in inh. neurons at V_{rest}. Inh. synaptic weights are determined by the factor g:

$$g = \frac{J^i \tau^i \left| V_{rest} - V_{rev}^i \right|}{J^e \tau^e \left| V_{rest} - V_{rev}^e \right|}.$$

For $g = 1$, the peak amplitude of an IPSP at resting potential of exc. neurons is 0.055 mV and 0.088 mV for inh. neurons.

We explore the dynamical phase space via numerical network simulations. Simulations were performed for v_{ext} ranging from 9 to 12 KHz (in steps of 0.5 KHz), and g ranging from 2.5 to 6 (in steps of 0.5), see Figs. 4 and 5. For each pair (v_{ext}, g) a simulation comprehends 2 s simulated time. To avoid transient effects, the first 500 ms are excluded from the analysis. Temporal precision of integration is 0.1 ms, all simulations are performed with NEST/PyNN (Gewaltig and Diesmann, 2007).

2.1. Phase space analysis

To describe and analyze the activity dynamics of the network, we compute the following observables and measures: the mean firing rate per neuron *FR* (based on time bins of 1 ms length), the mean free membrane potential V_m (Kuhn et al., 2004), and the mean change in total conductance *G*. These observables provide a general description of the neurons' activities and their dynamical state, they are directly related to the dynamical properties of a neuron. Due to the fact that we deal with different types of neurons, these quantities are calculated separately with respect to exc. and inh. neurons.

The correlation coefficient *CC* and Fano factor *FF* characterize the amount of synchrony in neuronal spiking patterns. The former, for a pair of neurons i, j, is defined as

$$CC(n_i, n_j) = \mathrm{cov}(n_i, n_j) \Big/ \sqrt{\mathrm{var}(n_i)\mathrm{var}(n_j)},$$

where n_i, n_j are the spike counts of neuron i and j, cov denotes their covariance, and var the variance. We estimate *CC* for time bins of 2 ms, averaging over as many (disjoint, randomly chosen) pairs as there are spiking neurons in the simulation. *FF* is calculated from the population activity, i.e., the variance of the firing rate divided by its mean (see e.g., Kumar et al., 2008b). For the Fano factor, we distinguish between the exc. and inh. population. We simplify the comparison of these two synchrony measures by computing $(FF - 1)/(N - 1)$ which is identical to *CC* for a population of N independent poisson processes in the limit of infinite observation time.

2.1.1. Regularity measures

To describe the irregularity in neuronal spiking we calculate the coefficient of variation

$$CV = \text{std}(ISI)/\mu(ISI),$$

where ISI stands for the inter-spike-interval distribution (based on time bins of 1 ms), and std and μ are the corresponding standard deviation and mean, respectively. For a regularly spiking neuron, we expect $CV = 0$, whereas $CV = 1$ for irregular poissonian spiking. In addition, we compute a local version of the coefficient of variation (Holt et al., 1996), CV_{loc}. This means computing the quotient of the standard deviation and mean of every two adjacent inter-spike-intervals and then averaging over all spike times of all neurons. Therefore, contrary to CV, CV_{loc} is relatively independent of slow variations in the mean spike rate.

The third measure to characterize the (ir)regularity in spiking is based on the Kullback–Leibler divergence (Kostal and Lansky, 2006; Koyama and Shinomoto, 2007):

$$CV_{KL} := \exp(-KL) \quad \text{with } KL = \sum P(ISI) \ln(P(ISI)/Q(ISI)) \qquad (1)$$

The idea is to estimate the difference between an unknown ISI distribution P(ISI) and a reference distribution Q(ISI). We use an exponential Q(ISI) as generated by poissonian spike trains with a mean μ(ISI). This again results in $CV_{KL} = 1$ for irregular poissonian spiking and $CV_{KL} = 0$ for regular spikes. Inserting an exponential distribution we can reduce Eq. (1) to

$$KL = -H_{isi} + \ln(\mu(ISI)) + 1 \quad \text{with entropy } H_{isi} = -\sum P(ISI) \ln(P(ISI)).$$

For any Gaussian P(ISI) this yields $CV_{KL} = \sqrt{2\pi/e}\,CV \approx 1.5CV$. Note that, instead of calculating CV_{KL} for each single neuron and then averaging, we use a 'collapsed' version (Fig. 5), i.e. we determine CV_{KL} from P(ISI) estimated from all neurons. Therefore, this measure characterizes the regularity of the population activity rather than the regularity in the spike trains of single neurons.

Finally, we calculate the spike entropy in time, $H = -\sum P(FR) \ln(P(FR))$. In general, entropy characterizes the amount of information present in a signal, or alternately, the disorder present in a system. Here, H is used as another estimate of the disorder in spiking, supplementary to the CV measures. It is computed separately for the exc. and inh. populations. We expect to see values that correspond to the CV measures: a small H for ordered spike times ($H = 0$ if only one bin is occupied, or for no spikes at all) and a larger H for random spiking ($H_{max} = 7.3$ for a uniform P(FR)).

2.1.2. Comparison of excitatory and inhibitory activities

The correlation coefficient, as well as the regularity measures are computed from all neurons. As it might be not appropriate to average over exc. and inh. neurons, we additionally calculate FF^e, FF^i to capture possible differences in terms of synchrony, as well as the spike entropies H^e, H^i to account for distinct regularities.[2] In order to investigate whether the two populations exhibit significantly different activities, we compare normalized differences between exc. and inh. neurons. Given a measure X, we determine $\max(X^e)$ and $\max(X^i)$ with respect to all input parameter pairs, and then calculate

$$\Delta_X(v_{ext},g) := \left|\frac{X^e(v_{ext},g)}{\max(X^e)}\right| - \left|\frac{X^i(v_{ext},g)}{\max(X^i)}\right| \Rightarrow D_{norm}(X) := \frac{1}{n}\sum_{v_{ext},g} \Delta_X(v_{ext},g),$$

where n is the number of all (v_{ext},g) pairs. This normalized difference $D_{norm}(X)$ gives a qualitative indication if X^e and X^i develop differently with respect to changes in (v_{ext},g).

3. Comparison of different regularity measures

In order to compare the three regularity measures described above, we generated several artificial ISI distributions and computed the corresponding CV, CV_{loc}, and CV_{KL} values. We consider unimodal Gaussians representing ISI distributions of nearly regular spiking neurons, i.e. similar inter-spike-intervals. In addition, we test with bimodal distributions, each generated by a simple mixture of two equally weighted single Gaussians. For these bimodal distributions, we examine the difference in the regularity measures for a varying distance between the single Gaussians that constitute them, as well as the effect of varying the relative heights of the single Gaussian peaks (Fig. 1).

Furthermore, we investigate the effect of the sample size on the three regularity measures. In the ideal case, there is an infinite number of samples for statistical analysis. In reality, however, a limited simulation (or experimental trial) time can result in very few spikes, i.e. very few inter-spike-interval values per neuron. We calculated CV, CV_{loc} and CV_{KL} for an exponential distribution in dependence of the number of samples used in generating the distribution (Fig. 2).

3.1. Results of comparing different regularity measures

The results of computing different regularity measures for the artificial ISI distributions are presented prior to the phase space analysis because of inconsistencies concerning these measurements. The bottom left part of Fig. 1 shows CV_{loc} and CV_{KL} for three artificial Gaussian ISI distributions with given $CV : \mu = 100$ and $\sigma_{1,2,3} = \mu/50$, $\mu/25$, $\mu/12.5$. This plot is representative for any other unimodal Gaussian with identical σ/μ relations. Increasing σ for a given μ leads to a proportional increase in all CV measures, as desired, indicating more irregular firing. CV_{KL} gives consistently higher values than the usual CV (due to $CV_{KL} \approx 1.5CV$, see Section 2.1.1) while CV_{loc} is only slightly larger than CV.

In case of bimodal artificial ISI distributions this general agreement vanishes. The top plot in Fig. 1 shows the results of calculating CV, CV_{loc} and CV_{KL} for two bimodal Gaussians with $\mu_1 = 50$ and $\mu_2 = 150$ combined to $\mu = 100$ on the left, and $\mu_1 = 150$ and $\mu_2 = 250$ combined to $\mu = 200$ on the right. Here, the usual CV yields incongruously large values. It is easy to see that $\sigma^2 = [2\sigma_1^2 + 2\sigma_2^2 + (\mu_1 - \mu_2)^2]/4$. For $\sigma_{1,2} \ll \mu$, this leads to $CV \approx |\mu_1 - \mu_2|/(\mu_1 + \mu_2)$. Thus, CV is practically independent of the $\sigma_{1,2}/\mu_{1,2}$ quotients, where $\mu_{1,2}$ and $\sigma_{1,2}$ denote the means and standard deviations of the two single mode P(ISI) that are combined to the bimodal one. Instead, CV is mainly inversely proportional to the distribution's mean, $\mu = (\mu_1 + \mu_2)/2$ (and proportional to the distance between the two peaks at μ_1 and μ_2). It does not capture the fact that the bimodal distribution has two well-separated sharp peaks, which we consider as regular spiking. In contrast, the other two measures yield small values that proportionally increase with $\sigma_{1,2}/\mu_{1,2}$, but are independent of μ. Such behavior appropriately reflects the underlying point process: a neuron with two preferred ISIs still fires regularly if the single mode P(ISI) are narrow enough.

The bottom right part of Fig. 1 indicates that the usual CV, contrary to CV_{loc} and CV_{KL}, strongly depends on the gap d between the peaks at $\mu_{1,2}$ of the bimodal distribution ($d = 130, 160, 190$). Likewise, only the CV values differ with respect to the weights of the single Gaussians: If the first peak at $\mu_1 = 50$ provides 75% of all samples (while $\mu_2 = 150$ provides 25%) the resulting mean of combined distribution is $\mu = 75$. If, vice versa, $\mu_1 = 50$ provides 25% of

---

[2] The high number of samples necessary to compute the CV_{KL} suggests avoiding the separation between exc. and inh. for this quantity.
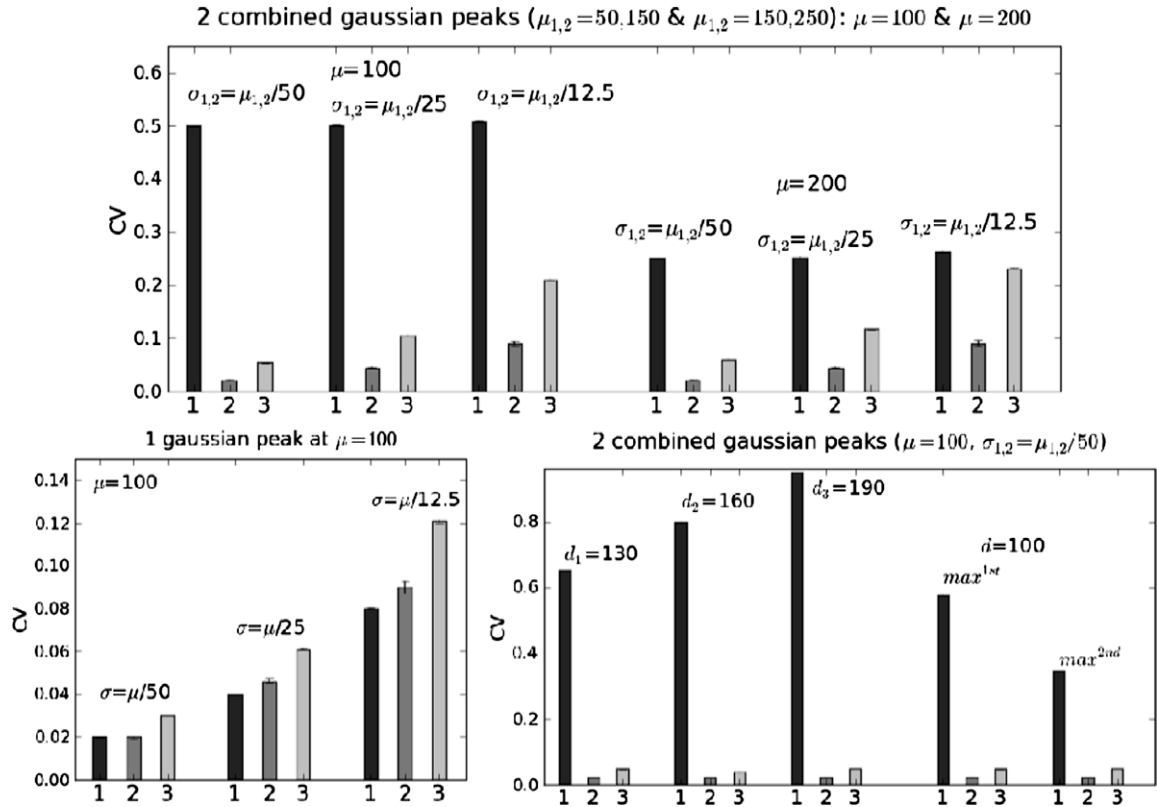
Fig. 1. Comparison of three regularity measures for several Gaussian distributions. On the *x*-axis a '1' represents the usual *CV*, a '2' is CV_{loc} and a '3' stands for CV_{KL}. The top row shows the results of calculating these measures for two bimodal distributions. Each of them is a combination of two Gaussians with a distance of 100 between the two peaks of the single distributions at μ_1 and μ_2. For comparison, the left bottom figure shows *CV*, CV_{loc}, CV_{KL} of unimodal Gaussian distributions. The right bottom figure shows the measures for bimodal distributions with different distances between the peaks of their single Gaussians. In addition, it compares the regularity measures for two bimodal distributions with equal distance between their peaks but different heights. Each data point is determined from an ensemble of 30 realizations.
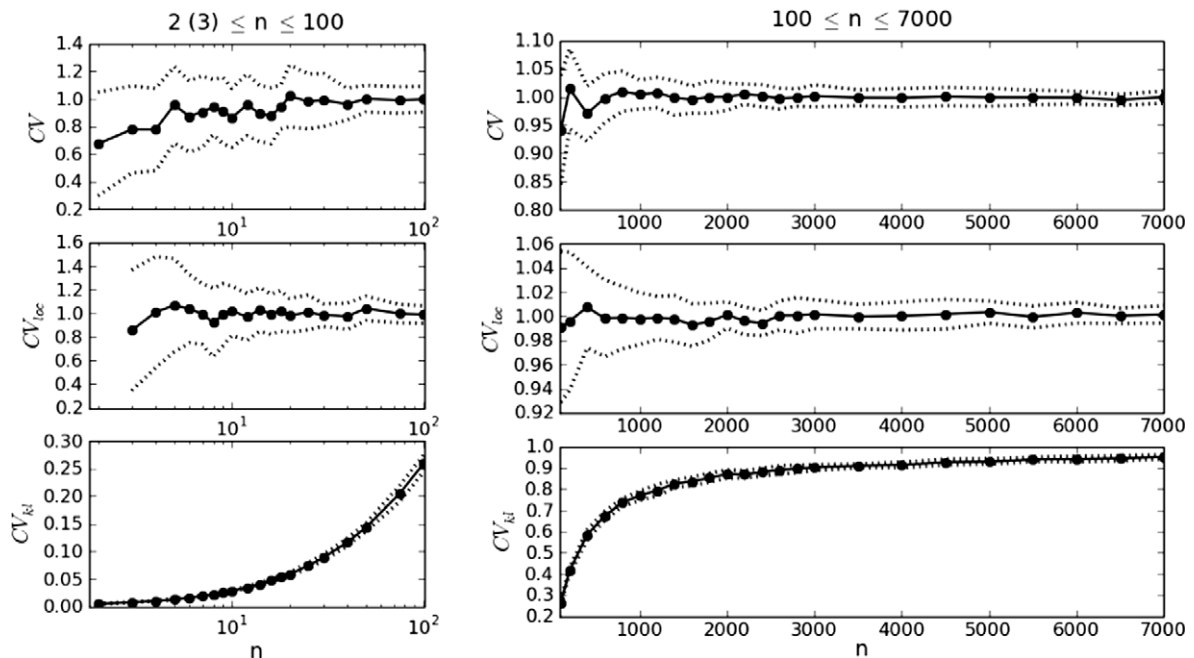

Fig. 2. Mean and standard deviation of three regularity measures for an exponential distribution ($\mu = 100$) in dependence of the number of samples n used to generate the distribution: The results for few samples are shown on the left (logarithmic *x*-axes); the right part shows the results for larger sample sizes (linear *x*-axes). Top row displays the usual *CV*, middle and bottom row the results of computing CV_{loc} and CV_{KL}. Each data point is determined from an ensemble of 30 realizations.

all samples, it is $\mu = 125$ and thus *CV* is 5/3 times larger in the first case. Such behavior is inappropriate in terms of characterizing the

regularity in spiking neurons: neither the distance between the preferred ISIs nor their weights should matter.

Fig. 2 shows the resulting CV, CV_{loc} and CV_{KL} values for artificial exponential ISI distributions typical for poissonian spike trains, i.e., ideally, all measures should be equal to one. The most striking observation is $CV_{KL} \ll 1$ for $n \lesssim 3000$, where $CV_{KL} = 0.9$. Thus, we determine P(ISI) from the ensemble of *all* neurons to compute the CV_{KL} measure. Likewise, but clearly less pronounced, the standard CV exhibits values smaller than one in case of smaller sample sizes $n \lesssim 100$, and $CV_{loc} < 1$ for $n \lesssim 4$. Concerning the standard deviations (computed from 30 realizations), CV_{KL} exhibits the smallest variations while CV_{loc} and CV show comparably large fluctuations, in particular for $n \lesssim 100$.

4. Results of the phase space analysis

The phase space of a network characterizes its activity dynamics depending on the input parameters. Varying the external input rate, v_{ext}, and the ratio between the strength of exc. and inh. synaptic weights, g, we now describe the results derived from the network simulations elaborated in Section 2. First, we show a choice of exemplary raster plots that captures the possible activity states. Second, we present the phase space, i.e., the results of calculating the observables and measures introduced in Section 2.1 for all parameters. On the basis of our findings, we classify different dynamical states and compare them to those described in previous studies.

4.1. Characterization of possible dynamical states

Fig. 3 shows exemplary raster plots (each row of dots represents the spike times of a certain neuron) of nine carefully chosen points in the phase space, marked by roman numerals in Figs. 4 and 5. For each raster plot we additionally present the mean firing rate over time $FR(t)$ and the corresponding ISI distribution, both from the population of all neurons. Here, a distinction between exc. and inh. neurons is not necessary because their raster plots exhibit (nearly) identical spike patterns. On the top left (I: small g, large v_{ext}) all neurons fire synchronously at very high rates leading to thin vertical stripes. The ISI distribution shows a narrow, very pronounced peak at very short inter-spike-intervals, indicating regular firing. We adopt, here and in the following, the notation in Brunel (2000) and Kumar et al. (2008a) where this behavior is called 'SR' state, for *synchronous regular* spiking. More specifically, this is a 'SR$_{fast}$' state. For slightly lower v_{ext} (IV) or slightly larger g (V) the raster plots exhibit broad vertical stripes corresponding to the maxima in the firing rate. The corresponding ISI distributions are bimodal, again with a pronounced peak for very small ISI lengths, but a second peak at about 100 ms (from the periodicity in $FR(t)$). We classify this spike pattern as 'SR$_{slow}$' (Brunel, 2000; Kumar et al., 2008a). Characteristic for both SR states is the occurrence of a time interval with no spikes at all. The length of this interval is approximately 8 ms in SR$_{fast}$ and up to 50 ms in SR$_{slow}$.

In contrast, on the bottom right (IX: large g, small v_{ext}), all neurons fire at fairly low rates with uncorrelated spike times and an exponential ISI distribution. Such behavior is called 'AI' state, i.e., *asynchronous irregular* spiking. Increasing v_{ext} combined with comparably high inhibition (III, less so in VI) leads to *synchronous irregular* firing patterns, a state called 'SI'. The corresponding ISI distributions are perturbed exponential ones. Compared to SR states the firing rates are low, and the neurons fire significantly less synchronously.

Various mixtures exist between these states, e.g., VII, VIII or II, which we classify into the following two categories: For intermediate values of g and v_{ext} the network dynamics may change from AI to SR$_{slow}$ and then, after a period of no spikes, back to AI and so forth (V, VII), not necessarily periodically. The smaller v_{ext} and

the higher g, the longer are the AI periods. Generally, it takes 20 up to 40 ms until the AI spiking accumulates to a SR$_{slow}$ activity burst which usually lasts for approximately 25–45 ms. In some cases (VIII) AI firing dominates, and is only occasionally disrupted by a SR$_{slow}$ burst. Another mixed state occurs for $g = 2.5$ and, more pronounced, for $g = 4$. Here, we observe mainly SR$_{slow}$ firing, but at the end of some activity maxima, one (IV, for $g = 2.5$) or several (II, for $g = 4$) SR$_{fast}$ bursts appear. For $g = 4$ in combination with $v_{ext} > 11$ KHz some SR$_{fast}$ intervals last for 20–100 ms.

4.2. Results of the phase space measures

Figs. 4 and 5 present an overview of the whole phase space. The labels in Fig. 4, top-left, refer to the states described above. The observables in Fig. 4 and two of the measures in Fig. 5 are determined for exc. neurons.[3] In general, the mean firing rate, the mean free membrane potential, the changes in conductances, and their standard deviations exhibit a similar behavior with respect to the input parameters. Maximal values occur for low inhibition combined with high input rates, and minimal values for large g and small v_{ext}. $V_m^{e,i}$ is exceptional for ($g \sim 3, v_{ext} \geqslant 10.5$ KHz) with minimal values but maximal fluctuations. Probably, this behavior is caused by the relatively long quiet periods and the following transition to high firing rates, typical for the SR$_{slow}$ state. In case of $v_{ext} \lesssim 10$ KHz and also for ($g > 3.5, v_{ext} \geqslant 10.5$ KHz), the regime classified as AI state, $V_m^{e,i}$ weakly fluctuates (small std(V_m)) about 5 mV below the threshold V_θ. This is in good agreement with (Kumar et al., 2008a). Membrane conductances are increased by a factor 1.2–6 relative to the membrane conductance at rest for exc. neurons. For inh. neurons the factor is in the range of 1.2–5. Correspondingly, this leads to a reduction of $\tau_{rest}^e = 10$ ms to 2–8 ms and of $\tau_{rest}^i = 6.7$ ms to 1.2–5.6 ms. These values are also not too far from Kumar et al. (2008a).

The SR$_{fast}$ state only exists for very high $v_{ext} \gtrsim 10.25$ KHz in combination with very low $g \leqslant 2.5$. It has an exceptionally high $FR^{e,i}$, a free membrane potential very close to the threshold, and a huge increase in $G^{e,i}$. Likewise, the corresponding fluctuations are large, see Fig. 4, bottom. Our SR$_{fast}$ state corresponds to the SR$_{slow}$ state in Kumar et al. (2008a) with about 11 maxima in $FR(t)$ per 100 ms. The SR$_{slow}$ state in Kumar et al. (2008a), however, differs from our results: Both time intervals of high firing and intervals with no spikes are much longer in our simulations. In addition, prior to the maxima in $FR(t)$, we often observe irregular spiking which then switches into a burst of activity, e.g., in raster plots IV, V, VII and VIII. Likewise, the spike pattern of what we call SI state (plots III, VI) is very different from Kumar et al. (2008a). In our simulations the synchrony of SR$_{slow}$ and SI is at a much larger time scale, around 80 ms rather than 9 ms.

Fig. 5 shows the results of measuring synchrony and regularity in neuronal spiking. CC and FF^e are in good agreement and confirm the findings described above: maximal values $CC > 0.4$ in the SR$_{fast}$ state ($g = 2.5, v_{ext} \approx 10.5$ or $v_{ext} \gtrsim 11.25$ KHz), a range with $CC \gtrsim 0.1$ indicating synchronous activity in the SR$_{slow}$ state, and a large region with asynchronous firing in case of low input rates or high inhibition. To identify what we called an SI state for ($g \gtrsim 4.5, v_{ext} \gtrsim 10.75$ KHz), we have to consider a higher resolution, see Fig. 6, left. A horizontal border ranging from $v_{ext} = 10.75$ KHz at $g = 4.5$ up to $v_{ext} = 11.5$ KHz at $g = 6$ separates the AI from the SI state. Compared to the SR states, however, $CC \gtrsim 0.01$ is rather small. Thus, other than reported in Kumar et al. (2008a), our SI state is not as well-defined.

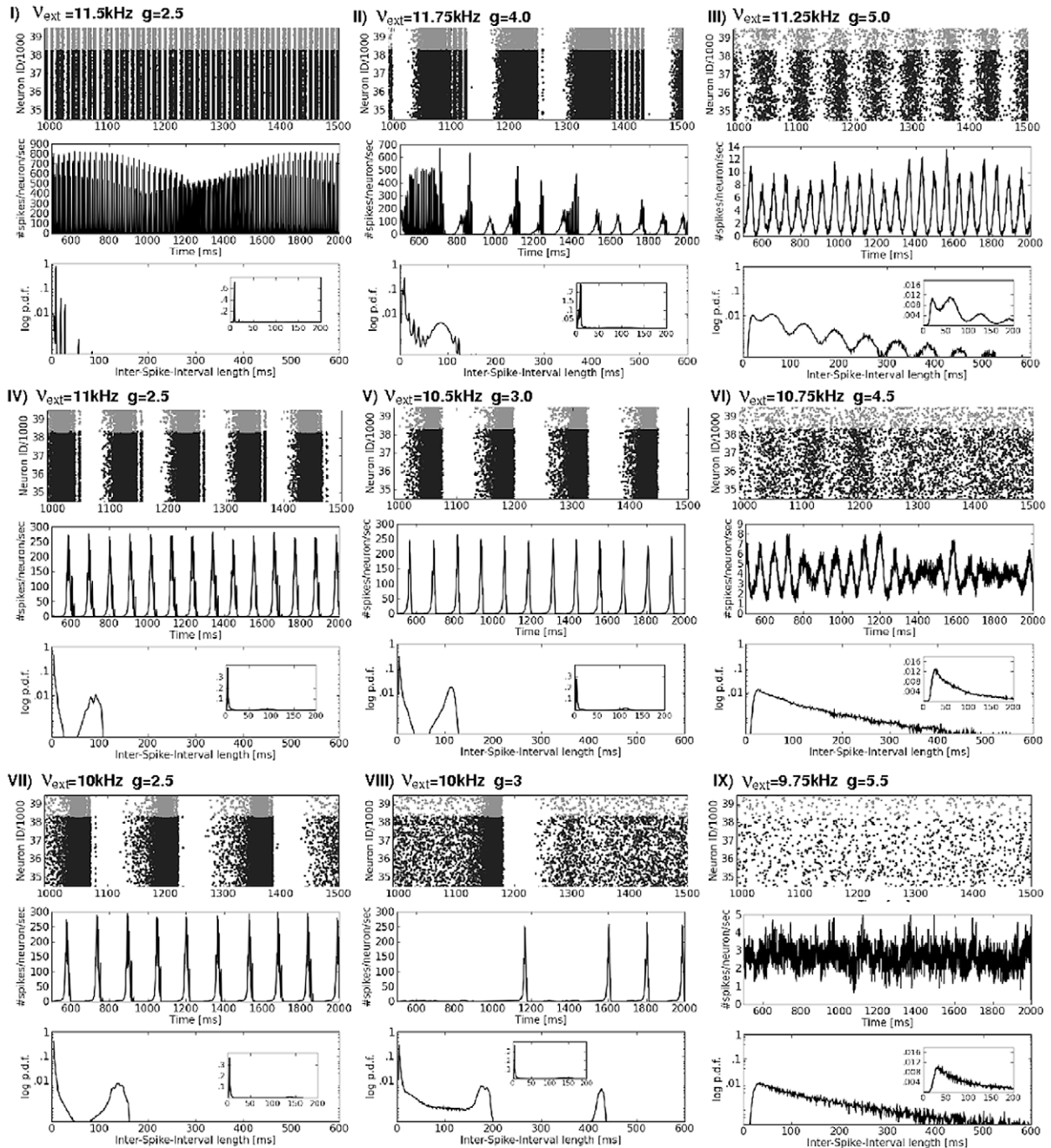[3] The corresponding plots for the inh. population are not shown, but are very similar.

Fig. 3. Representative network simulations (I)–(IX): raster plot sections (top) with corresponding firing rates (middle, last 1.5 s of simulation time), and ISI probability density distributions (bottom, semilogarithmic plots with a zoom-in with linear axes). In the raster plots, gray dots represent inh. spikes, and black dots represent exc. spike times while the other two plots do not distinguish between exc. and inh. neurons. The plots are ordered and numbered according to their occurrence in the phase space: On the top left synchronous regular firing dominates due to low inhibition (small g) and high input rates. On the bottom right, there is asynchronous irregular firing due to a higher inhibition (large g) and lower input rates. The corresponding V_m, G, FR, CC, FF, CV values are marked by roman numerals in Figs. 4 and 5.

The regularity measures presented in Fig. 5 yield inconsistent results: We expected $CV \sim CV_{loc} \approx 1$ for the AI state but found mostly $0.6 \lesssim CV \lesssim 0.8$ or even $CV \approx 0.4$ for $v_{ext} < 9.5$ KHz, and $CV_{loc} \approx 0.8$. In this latter range, the firing rates are very low, $FR < 5$ Hz, resulting in on average less than 7 spikes per neuron per 1.5 s simulation time. This led to the analysis presented in Section 3 (Fig. 2) which confirms the underestimation of CV in case of too few events. For the SR$_{fast}$ state, all regularity measures clearly indicate regular spiking neurons ($CV \sim CV_{loc} \sim CV_{KL} < 0.1$). For the SR$_{slow}$ state we find $CV > 1$. This clearly contradicts the regular appearance of the spike patterns in the raster plots, as well as the shape of the corresponding ISI distributions. They sport a bimodal P(ISI) with one strongly preferred small inter-spike-interval, and a second, larger and less frequent one. A well-known solution for bimodal P(ISI) is to calculate CV_{loc} instead of CV (Holt et al., 1996), see Section 2.1.1. This works quite well for the artificial P(ISI) in Section 3.1, but not for the simulated data as presented in Fig. 5. Furthermore, as expected from Section 3.1, $std(CV_{loc})$ is large (see Fig. 6, middle-left) compared to $std(CV) < 0.1$ for most input parameters and $std(CV)_{max} \approx 0.26$. Therefore, we additionally cal-
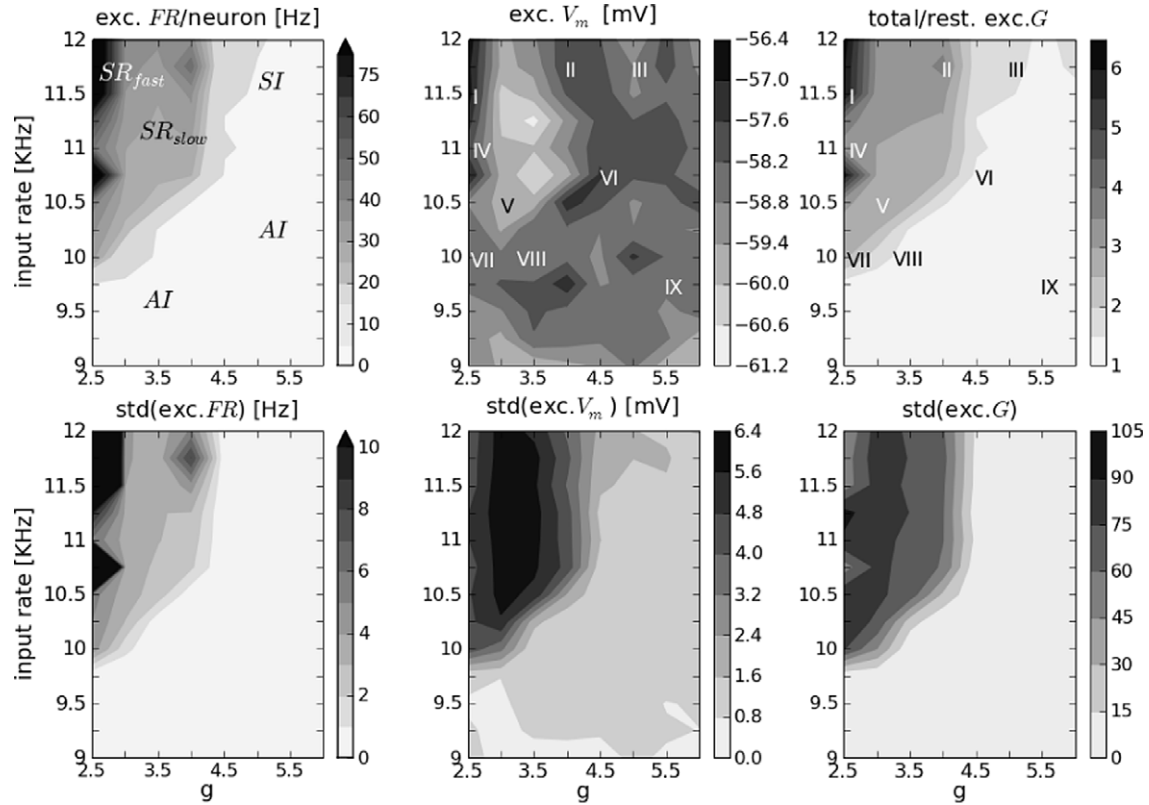
Fig. 4. Phase space analysis, part one: Shown are the mean FR ($FR^e_{max} = 105.6$ Hz), the mean free V_m and the mean change from resting to total conductance G of the exc. population for varying g (x-axis) and v_{ext} (y-axis). The bottom row shows the corresponding standard deviations: std(FR^e)$_{max} = 55.8$, std(G^e) describes the variations in the measured G^e values ($G^e_{min} = 4.8$ nS, $G^e_{max} = 153.5$ nS). The corresponding values for the inh. population are: $FR^i_{max} = 66.4$ Hz, $V^i_{m,min} = -61$ mV, $V^i_{m,max} = -58$ mV, and the mean change from resting to total conductance of the inh. population ranges from 1.15 to 5.1. The inh. standard deviations are std(FR^i)$_{max} = 19.5$, std$\left(V^i_m\right)_{max} = 5.4$, std($G^i$)$_{max} = 53.9$ $\left(G^i_{min} = 3.14$ nS, $G^i_{max} = 86.9$ nS$\right)$. The roman numerals indicate the specific (v_{ext}, g) pairs for which the corresponding raster plots, firing rates, and ISI distributions are shown in Fig. 3.

culated CV_{KL}. As this measure needs a large sample size (Fig. 2), we determine it from the P(ISI) of the population of all neurons ('collapsed'). These results finally agree with our expectation from the exemplary raster plots and ISI distributions in Fig. 3 for the phase space: irregular spiking occurs for low input rates, as well as for high v_{ext} combined with high inhibition.

4.3. Comparison to previously described phase spaces

We are now in a position to compare our phase space to previously published work. In networks with current-based synapses (Brunel, 2000) the transition from high to low activity states takes place for a certain amount of recurrent inhibition and is independent of the input rate. This corresponds to a *vertical boundary* in the corresponding phase space at $g = 4$. Kumar et al. (2008a) state that, for conductance-based synapses, the phase boundary changes. The range of interest for the recurrent inhibition is shifted to $g \in [1, 3]$. High activity states (SR) with more than 60 spikes/s per neuron, occur only for high v_{ext} nearly independent of g. This corresponds to a *horizontal boundary* in the phase space. Their border between SR$_{fast}$ and SR$_{slow}$ is approx. $2 \lesssim g \lesssim 2.5$. Their SI state appears only in case of v_{ext} slightly lower than that for SR states combined with $g \gtrsim 2.5$. Moreover, Kumar et al. (2008a) found, in contrast to Brunel (2000), no state with *asynchronous regular* (AR) activity – neither did we.

In terms of the mere occurrence of SR, AI and SI states, our results agree with (Kumar et al., 2008a). Yet, our SR and SI activities exhibit a larger time scale, as well as lower FR in case of SR$_{slow}$ activity. The phase space of our network model comprises

$g \in [2.5, 6]$, i.e., larger values than in Kumar et al. (2008a), more similar to Brunel (2000). We found a sharp *vertical boundary* at $g < 3$ separating the range where a pure SR$_{fast}$ state can exist from the SR$_{slow}$ state. In contrast to Kumar et al. (2008a) we observe no direct transition from AI to SR$_{fast}$. Likewise, Figs. 4 and 5 show no extended horizontal boundary, as indicated by Kumar et al. (2008a). The occurrence of synchronous regular spiking depends on both g and v_{ext}: the higher the external input rate the more inhibition is necessary to stay in the AI state. In particular, for $g \gtrsim 4.5$ we observe no regular spiking and no high firing rates, independent of v_{ext}. At about $v_{ext} \gtrsim 11$ KHz the network dynamics turns into the SI state with $FR \lesssim 10$ Hz, i.e., a low activity state.

As mentioned before, we observe 'mixed' states. The network activity changes within one simulation run between AI and SR$_{slow}$. This indicates a gradual transition from SR$_{slow}$ to AI instead of a sharp boundary. Likewise, the SR$_{slow}$ state may contain bursts of SR$_{fast}$ activity patterns. Nevertheless, the transition from pure SR$_{fast}$ activity to SR$_{slow}$ is much sharper than the AI to SR$_{slow}$ one. Such mixed states, or the *coexistence* of different phases, especially in a dynamic sense, have not been mentioned before.

4.4. Comparison of excitatory and inhibitory activities

The observables G, FR and V_m are computed separately for the exc. and inh. population. In the SR$_{fast}$ state, FR^e may become approximately twice as large as FR^i. The same statement holds for the directly measured $G^{e,i}$, but not in terms of the change from resting to total conductance. The maximum increase (for SR$_{fast}$) is 6.2 for exc. neurons versus 5.1 for inh. ones. V^e_m is, in general, closer
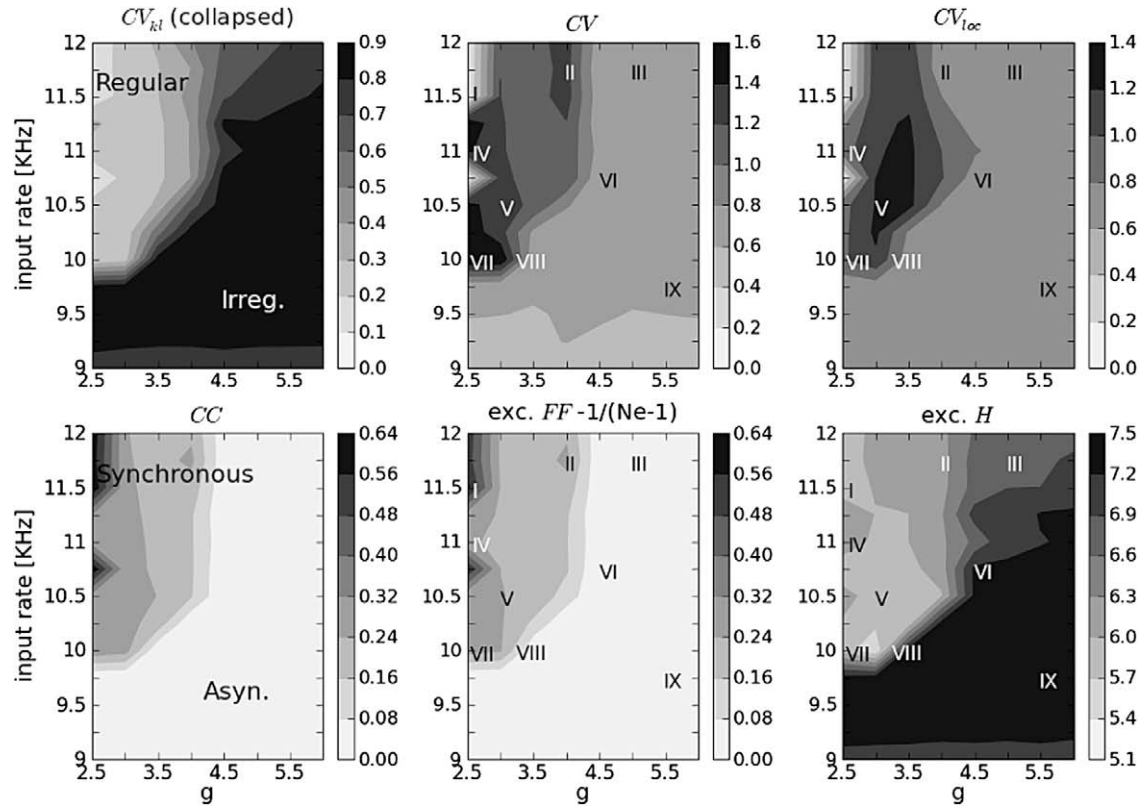
Fig. 5. Dynamical state space analysis, part two: The top row shows three measures of the regularity in neuronal spiking: the mean CV_{KL}, CV_{loc}, and CV, averaged over the exc. and inh. populations. The bottom row indicates two measures for synchrony in neuronal spiking: The correlation coefficient CC (averaged over exc. and inh. neurons) and the Fano factor FF of the exc. population (normalized to be comparable to CC). The plot on the bottom right indicates the spiking entropy H of the exc. population. The corresponding values for the inh. population are: $FF^i_{max} = 0.41$, $H^i_{min} = 4.86$, $H^i_{max} = 7.26$. Again, all measures are given for varying g (x-axis) and v_{ext} (y-axis). The roman numerals indicate the specific (v_{ext}, g) pairs for which the corresponding raster plots, firing rates, and ISI distributions are shown in Fig. 3.
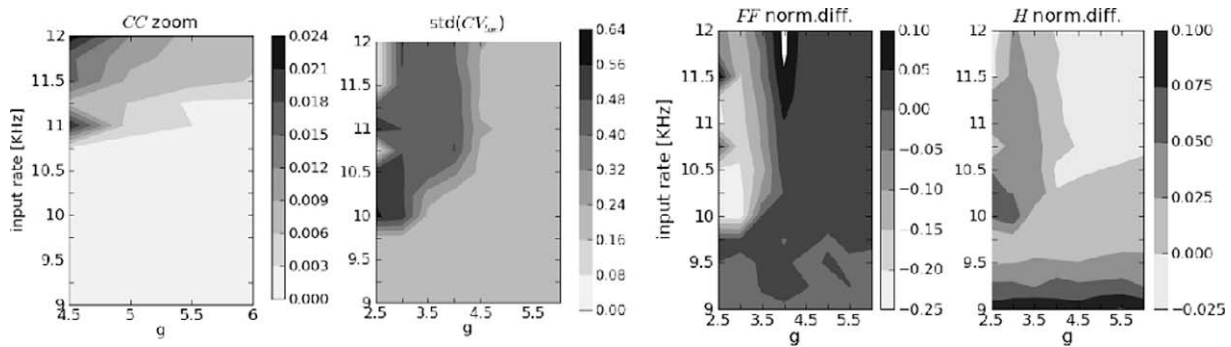

Fig. 6. Details of the phase space analysis. Left: CC for a limited range of g and a cut-off in the color scale. Middle-left: Standard deviation of CV_{loc}. The two plots on the right show the normalized difference between the exc. and inh. population for the Fano factor Δ_{FF} and the entropy Δ_H, again for varying g (x-axis) and v_{ext} (y-axis).

to the firing threshold than V^i_m, at maximum about 2.5 mV above V^i_m. The obvious conflict between considering fast spiking inh. neurons (vs. regular spiking exc. ones) and measuring higher exc. firing rates is reconciled by reducing the input rates for inh. neurons. This will be discussed in more detail in Section 5. The measures CC, CV, CV_{loc} and CV_{KL} do not distinguish between the two populations. In order to capture possible differences in terms of synchrony and/or regularity in spiking, we additionally calculated FF^e, FF^i and the spike entropies H^e, H^i. Fig. 6 shows the normalized differences introduced in Section 2.1.2 for the Fano factor, for which $D_n(FF) = 0.04$, and for the spike entropy with $D_n(H) = 0.03$. The other measures yield even smaller normalized differences: $D_n(FR) = 0.014$, $D_n(V_m) = 0.015$, and $D_n(G) = 0.011$.

Thus, in principle, the exc. and inh. populations exhibit a very similar behavior with respect to variations of (v_{ext}, g), even though their absolute FR^e, FR^i values are (very) different.

5. Discussion

We analyzed the changes in the activity dynamics of a cortical network with conductance-based synapses that are induced by the following assumptions: a spatially extended network architecture with distance dependent delays, the distinction between fast spiking inh. and regular spiking exc. neurons, and a very sparse global connectivity that comprehends specific connection proba-

bilities for different synaptic types. These changes lead to both, different activity patterns and modified phase transitions.

The general appearance of high SR activity for large input rates combined with low inhibition and weak AI activity for low v and small g matches the observations of previous studies. The general properties of the AI state, e.g., a membrane potential that fluctuates a few millivolts below threshold, are in line with (Kumar et al., 2008a). They are also in good agreement with in vivo intracellularly recorded neurons (Destexh et al., 2003). Likewise, our changes in membrane conductances and the corresponding reduction of membrane time constants in the AI state are in line with in vivo physiological observations (Destexh et al., 2003). Other than reported in Kumar et al. (2008a) and Brunel (2000) the occurence of strongly oscillating SR_{fast} states is limited to a small parameter range. Note that such highly synchronized and regular firing is far from physiological observations in healthy animals. Instead, we mainly observe distinct activity patterns with slower changes in the firing rate and bimodal ISI distributions, i.e., SR_{slow} states. In particular, our phase space reveals a parameter range where the network activity may dynamically switch from AI to SR_{slow} and then back to AI, and so forth. Likewise, there is a certain parameter range where SR_{slow} bursts contain SR_{fast} fast oscillations. This behavior can be considered as the coexistence of two states, a bistable regime, which has not been reported in Kumar et al. (2008a) and Brunel (2000). Alternately, the SR_{slow} state may simply represent the transition from AI to SR_{fast}. Note that Roxin et al. (2005) show that the phase diagram of a simpler 1D network model strongly depends on both conduction delays and spatial modulation of synaptic weights. Including the latter two features gives rise to various new activity patterns. Recalling the large distance-dependent conduction delays in our model, this might explain the coexistence of phases we described.

In addition, we found other phase boundaries between high and low activity states: Contrary to the predominantly v-dependent *horizontal boundary* in Kumar et al. (2008a) our simulation results reveal a prevailing *vertically oriented border*, i.e., g-dependent, between SR and AI activity. This is rather typical for networks with current-based synapses (Brunel, 2000) where the border separating SR from AI is $g_{crit} \simeq 4$. In Kumar et al. (2008a), $v_{ext,crit}$ determines the transition from low to high activity: If the input is larger than $v_{ext,crit}$ the network switches into SR_{fast} ($g \lesssim 2$) or SR_{slow} ($g \gtrsim 2$). We found no direct transition from AI to SR_{fast}, instead, we observe the following three boundaries: one at $g < 3$, separating the possibility of pure SR_{fast} from SR_{slow} activity, and another one at about $3.5 \lesssim g \lesssim 5$ capturing the transition range between SR_{slow} and AI or SI states. For $v_{ext} \lesssim 10$ KHz only AI or SI activity occurs.

5.1. The ratio between external and internal connections

We did not address the absolute values of v_{ext}, neither the corresponding number of input synapses, nor their firing rates. Likewise, we used a reduced input rate for inh. neurons without further explanation. Recall that Mehring et al. (2003), Kumar et al. (2008a,b) focus on local connections within a small cortical patch (around 1 mm side length), where approx. 10% of all possible connections are realized. Then, the external input rate v_{ext} represents synapses from neurons outside the model. We consider a larger piece of cortex (25 mm²) with fewer internal connections ($c \approx 0.0153$). On one hand, we are thus not limited to local dynamics, but on the other hand, we have an unrealistically low density of neurons. Therefore, while one fraction of v_{ext} represents synapses from neurons outside the network model, another fraction of our external input rate compensates for the missing internal synapses.[4]

---

[4] Similar to Kumar et al. (2008a,b), and Brunel (2000) we neglect inh. inputs and assume them integrated into the external exc. rate.

Kumar et al. (2008a) consider approximately 5000 internal synapses and 4000 external input connections per neuron with a firing rate of $2.5 \leqslant v_{ext} \leqslant 7$ Hz per input connection. This is difficult to compare with approx. 750 internal synapses per neuron in our network model. According to Binzegger et al. (2004) the average number of synapses a pyramidal neuron in layer 2/3 of cat primary visual cortex receives from other layer 2/3 pyramidal neurons is approx. 3500. In addition, there are about 1000–1500 external exc. inputs. Therefore, our external input rate represents around 4000 synapses, 2750 internal and 1250 external ones. For $9 \leqslant v_{ext} \leqslant 12$ KHz this means an average input firing rate between 2 and 3 Hz per input connection, which seems a bit on the low side.

The internal synapses are based on specific connection probabilities, as described in Section 2. For instance, the probability for an internal exc. input connection to another exc. neuron is 0.711/0.78 = 0.911 (due to a higher probability for ee synapses than expected for purely random connectivity). The probability for an internal exc. input connection to another inh. neuron is smaller, namely 0.0996/0.22 = 0.453. Accordingly, inh. neurons should receive only approx. half of the exc. external input that represents the missing internal synapses. Concerning the external inputs from outside the cortical patch (e.g., from another cortical layer or white matter connections from another cortical area) we assume no preferences, i.e., randomly chosen targets. Depending on the numerical relation between input from inside and outside the network model, the factor f_i to reduce the input rate of inh. neurons is $0.5 < f_i < 1$. We chose $f_i = 0.66$ for practical reasons: Assuming $f_i < 0.64$ results in strongly synchronized network activity with hardly any AI dynamics. In contrast, for $f_i > 0.68$ we hardly observed any SR state. Interestingly, with respect to the discussion above, $f_i = 0.66$ corresponds exactly to reducing the part of v_{ext} representing internal synapses for inh. neurons to 50% of that of exc. neurons.

Since the network dynamics strongly depend on f_i, we discuss another possibility to justify the assumption of $f_i = 0.66$. Obviously, f_i depends on the neuron parameters that determine their spike rates. As explained in Section 2 the EPSP peak amplitudes at resting potential for exc. neurons are approx. 0.61 times smaller than for inh. cells, but have a larger time constant. In order to compare the spike rates of exc. and inh. neurons, we investigated the number of incoming action potentials necessary to produce a spike (n_{spk}), in dependence of the integration time: For instance, exc. cells need 166 spikes and inh. neurons only 90 spikes within 1 ms to produce a spike. Within 40 ms, exc. cells need 530 spikes and inh. neurons 380 spikes. Thus, the numeric relation $\left(n^i_{spk}/n^e_{spk}\right)$ is between 0.54 and 0.72, a range that contains the factor $f_i = 0.66$.

5.2. Different regularity measures

Due to difficulties in characterizing the regularity in neuronal spiking, we considered three different measures which we then compared by means of artificial ISI distributions. The typical CV malfunctions for bimodal distributions. CV_{loc} performs well for artificial multimodal distributions. For our simulation data, however, the CV_{loc} values are not in accordance with what we classify as (ir)regular – based on a visual inspection of the spike trains and the corresponding ISI distributions. Moreover, some simulations do not provide enough spikes for statistical analysis. Therefore, we used another measure, CV_{KL}, and applied it to the ISI distribution for the population of all neurons. Another possibility would be to extend the simulation time. We refrain from doing so, because in biological experiments the recording time is also limited. Too few spikes are presumably the reason for $CV \approx CV_{loc} \approx 0.6$ instead of $CV_{loc} \approx 1$ in case of AI activity. The question remains why $CV_{loc} \approx 1$ instead of CV_{loc} near zero for SR_{slow} states. One indication is the comparably high std(CV_{loc}), another is-

sue might be the still rather low firing rate. From another point of view, this could reflect an intrinsic property of our simulation data: At the population level, spiking is relatively regular, as indicated by the ISI distributions and $CV_{KL} \lesssim 0.3$, while it might be more irregular with respect to single neurons.

6. Summary and conclusions

To summarize, our network modifications induce clear changes in the phase space. We require a new regularity measure to adequately describe different activity states. As the dynamical behavior strongly depends on the network parameters, it is necessary to identify the most important ones, together with their critical range, i.e., the phase space region where the network dynamics switch from one state into another. We found a significantly different critical range than (Kumar et al., 2008a). In addition, we found 'mixed' states, which is presumably important in terms of stability analysis. Assume that the network is tuned to be in the AI state that represents cortical background activity. Then, providing an external stimulus, the corresponding information may be processed within this AI activity, but it may also turn the network into another state, e.g., a coexistence of AI and SR activity. In particular, the properties V_m, $\text{std}(V_m)$ and the changes in G of our AI–SR$_{slow}$ activity are more similar to the AI than to the SR$_{fast}$ state, i.e., similar to cortical activity. Only our SR$_{fast}$ state clearly differs from healthy cortical dynamics.

We conclude that including only a few more realistic parameters to simulate cortical network dynamics significantly affects the resulting activity patterns. The assumption of local couplings or a distant dependent connectivity might have an even larger effect. Thus, this study can only be a first step into the direction of improving the analysis of cortical network dynamics.

Acknowledgements

References

Binzegger, T., Douglas, R.J., Martin, K.A.C., 2004. A quantitative map of the circuit of cat primary visual cortex. J. Neurosci. 39 (24), 8441–8453.
Binzegger, T., Douglas, R.J., Martin, K.A.C., 2007. Stereotypical bouton clustering of individual neurons in cat primary visual cortex. J. Neurosci. 27 (45), 12242–12254.
Brunel, N., 2000. Dynamics of sparsely connected networks of excitatory and inhibitory spiking neurons. J. Comput. Neurosci. 8 (3), 183–208.
Brunel, N., Wang, X.-J., 2003. What determines the frequency of fast network oscillations with irregular neural discharges? I. Synaptic dynamics and excitation–inhibition balance. J. Neurophysiol. 90, 415–430.
Buzas, P., Kovacs, K., Ferecsko, A.S., Budd, J.M.L., Eysel, U.T., Kisvarday, Z.F., 2006. Model-based analysis of excitatory lateral connections in the visual cortex. J. Comp. Neurol. 499, 861–881.
Destexh, A., Rudolph, M., Pare, D., 2003. The high conductance state of neocortical neurons in vivo. Nat. Rev. Neurosci. 4, 739–751.
Gerstner, W., Kistler, W., 2002. Spiking Neuron Models: Single Neurons, Populations, Plasticity. Cambridge University Press, Cambridge.
Gewaltig, M.O., Diesmann, M., 2007. NEST. Scholarpedia 2 (4), 1430.
Holt, G.R., Softky, W.R., Koch, C., Douglas, R.J., 1996. Comparison of discharge variability in vitro and in vivo in cat visual cortex neurons. J. Neurophysiol. 75 (5), 1806–1813.
Kostal, L., Lansky, P., 2006. Similarity of interspike interval distributions and information gain in a stationary neuronal firing. Biol. Cybern. 94, 157–167.
Koyama, S., Shinomoto, S., 2007. Inference if intrinsic spiking irregularity based on the Kullback–Leibler information. BioSystems 89, 69–73.
Kuhn, A., Rotter, S., Aertsen, A., 2004. Neuronal integration of synaptic input in the fluctuation driven regime. J. Neurosci. 24 (10), 2345–2356.
Kumar, A., Schrader, S., Aertsen, A., Rotter, S., 2008a. The high-conductance state of cortical networks. Neural Comput. 20, 1–43.
Kumar, A., Aertsen, A., Rotter, S., 2008b. Conditions for propagating synchronous spiking and asynchronous firing rates in a cortical network model. J. Neurosci. 28 (20), 5268–5280.
Mehring, C., Hehl, U., Kubo, M., Diesmann, M., Aertsen, A., 2003. Activity dynamics and propagation of synchronous spiking in locally connected random networks. Biol. Cybern. 88 (5), 395–408.
Muller, E., 2003. Simulation of high conductance states in cortical neuronal networks. M.Sc. Thesis, University of Heidelberg.
Nowak, L.G., Azouz, R., Sanchez-Vives, M., Gray, C.M., McCormick, D.A., 2003. Electrophysiological classes of cat primary visual cortical neurons in vivo as revealed by quantitative analyzes. J. Neurophysiol. 89, 1541–1566.
Roxin, A., Brunel, N., Hansel, D., 2005. Role of delays in shaping spatiotemporal dynamics of neuronal activity in large networks. PRL 94, 238103.
Tuckwell, H.C., 1988. Introduction to Theoretical Neurobiology, vol. 1. Cambridge University Press, Cambridge.
Voges, N., 2007. Statistical analysis of cortical networks based on neuroanatomical data. Ph.D. Thesis, Fakultät für Biologie, Albert-Ludwigs-Universität Freiburg.